SPECIAL ISSUE: NANOSTRUCTURED MATERIALS 2010

Electrodeposition of polyaniline–carbon nanotubes composite films and investigation on their role in corrosion protection of austenitic stainless steel by SNIFTIR analysis

V. Martina · M. F. De Riccardis · D. Carbone · P. Rotolo · B. Bozzini · C. Mele

Abstract Composite films of polyaniline (PANI) and carbon nanotubes (CNTs) were prepared by electrochemical co-deposition from solutions of the corresponding monomer containing two different kinds of CNTs. The first type was commercial (diameter = 110–170 nm, length = 5–9 μm) and the second one was home-made (diameter = 30 nm, length = 5–20 μm). The electrochemical behaviour of PANI–CNTs composite films was investigated with Cyclic Voltammetry and the surface morphology was analysed by Scanning Electron Microscopy (SEM). Subtractively Normalised Interfacial FT-IR procedure was used to investigate the presence of corrosion products when the films were deposited on stainless steel substrates and exposed to acid environment. The spectral investigations were utilised to understand the role of composite films in the corrosion protection and to discriminate the best performance CNTs.

Keywords Polyaniline · Carbon nanotubes · Electrochemistry · FT-IR

V. Martina · M. F. De Riccardis (✉) ·
D. Carbone · P. Rotolo
ENEA Technical Unit of Materials Technology
of Brindisi, SS.7 Appia Km 706, 72100 Brindisi, Italy
e-mail: federica.dericcardis@enea.it

B. Bozzini · C. Mele
Dipartimento di Ingegneria dell'Innovazione,
Università del Salento, Via Monteroni, 73100 Lecce, Italy

Introduction

In the last decade, conducting polymers (CPs) have arisen wide interest as electrode materials and they have reached a state of development that allow their use in various applications such as sensors, membranes for the separation of gas mixtures, corrosion protection, and so forth (Skotheim et al. 1998). Among the CPs, polyaniline (PANI) has been one of the most studied because of its facile synthesis, electrical conductivity, low cost and environmental stability (MacDiarmid et al. 1987; MacDiarmid and Epstein 1995). It is characterised by a relatively wide potential stability, a reproducible synthesis and a well-behaved electrochemistry showing different domains of conductivities, which refer to different oxidation states of the polymer. Each oxidation state can exist in the form of its base or its protonated form (salt) by treatment of the base with an acid. Depending on the oxidation state and the degree of protonation, PANI can be either an insulator or a conductor with different conductivities (Stilwell and Park 1989; Huang et al. 1986).

Recently, several studies in the fields of new materials have introduced the possibility to use CPs as suitable matrices to disperse nanostructural elements, such as carbon nanotubes (CNTs). It has been shown that the introduction of CNTs into a polymer matrix can improve the electrical conductivity and the mechanical properties of the original polymer matrix (Wagner et al. 1998; Qian et al. 2000). Many

studies have optimised the preparation of CNTs–CPs composites and a large number of CNTs-based composites have been prepared. In this respect, the formation of PANI–CNTs composites has been discussed in literature, hypothesising different interaction mechanisms. Recent studies have shown that PANI could be used to functionalise and solubilise CNTs via formation of donor–acceptor complexes (see Scheme 1). In fact, CNTs should act as good electron acceptors, while PANI is a fairly good electron donor (Sun et al. 2001). The π-bonded surface of the CNTs may interact strongly with the conjugated structure of PANI, especially through the quinoid ring. Such selective interaction of the CNTs with the quinoid ring of PANI has been reported in literature (Zengin et al. 2002; Cochet et al. 2001). Moreover, the possible presence of functional groups on the CNTs' surface can favour a chemical interaction of both the monomer and the polymer during its generation (Peng et al. 2007).

PANI can be synthesised chemically or through electrochemical polymerisation. The electrochemical method is used more often because it is environmental friendly and presents several advantages. In fact, polymerisation media can be used repeatedly and polymerisation rate can be controlled by varying potential values.

In this article, PANI composite films containing two different types of CNTs were synthesised and characterised. Furthermore, the CNTs influence on the electrochemical properties of PANI was investigated. The synthesis of PANI–CNTs composite films was performed via electrochemical co-deposition onto electrode materials, so that the CNTs were incorporated in the PANI matrix during the electropolymerisation process. In other words, the formation of the composite occurred during the electrogeneration-deposition of the polymer just near the electrode surface, in a solution containing both CNTs and aniline. We intended to investigate the morphology and the properties of the composites films so obtained.

The main application of this kind of material could be in the field of anticorrosion protection in particular on ferrous alloys. Therefore, in this study, we studied the anticorrosive properties of PANI–CNTs composite coatings using combined electrochemical and spectroscopic techniques, such as in situ FT-IR. As known by the authors, we first reported on in situ electrochemical FTIR investigation performed at a stainless steel electrode.

Experimental details

All analytical-grade chemicals were purchased from Sigma-Aldrich and used as received, including Aniline monomer (analytical-grade). Two different types of CNTs were used in this study. CNT_c. (diameter = 110–170 nm, length = 5–9 μm) were purchased from Sigma-Aldrich. CNT_{hm} (mean diameter = 30 nm, length = 5–20 μm) were prepared by catalytic Thermal Chemical Vapour Deposition (TCVD) (Dikonimos et al. 2005). By SEM observation, CNT_{hm} resulted to be longer, less straight and with a lower diameter than that of CNT_c.

CNTs were purified by boiling in a solution of HNO_3 and HCl (3:1) for 1 h to dissolve any catalysts. CNTs were then washed with deionised water until pH 6 and then dried at about 70 °C. Triton X-100 has used as surfactant to disperse CNTs in water, since this prevents them from becoming aggregated for a long period.

Aniline polymerisation and composite formation were carried out in a conventional three-electrode cell. The working electrode was a carbon paper disk, having an exposed area equal to 1.1 cm^2. The counter electrode was a Pt wire and the reference electrode was an Ag/AgCl electrode (AMEL). For the films deposition, a PAR 273A potentiostat (Princeton
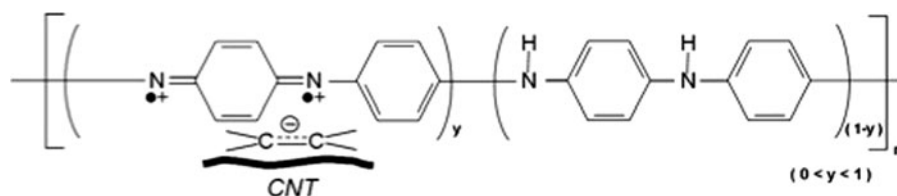
Scheme 1 Illustration of the interaction between PANI and CNTs

Applied Research, Oak Ridge, TN) in remote control was used. All the experiments were carried out at room temperature. Deionised water was used for rinsing electrodes and preparing solutions.

In order to deposit PANI and PANI–CNTs films on carbon paper and stainless steel substrates, 0.25 M aniline solutions in 1 M HCl and 0.5 M H_2SO_4, respectively, were used. In a typical experiment, CNTs dispersed in Triton X-100 were added to aniline solutions with different contents from 0 to $0.3\%_{v/v}$ (volume percent with respect to aniline solution).

The PANI–CNT composite films were deposited by cyclic voltammetry (CV) on carbon paper substrates, and by potentiostatic technique on stainless steel at potential 0.9 V versus Ag/AgCl, lower than that of steel oxidation. The morphology of the electrodeposited films was characterised using a FEG-SEM LEO 1530 microscope.

PANI and PANI–CNTs films were characterised electrochemically in 0.5 M H_2SO_4 solution that was deaerated with Argon gas for 10 min prior to use. Their potential efficiency in the corrosion prevention was studied by adding 10 mM $FeSO_4$ to sulphuric acid solution. In FT-IR measurements, a solution of H_2SO_4 50 mM and ethanol (50 vol%) was used. All experiments were done at room temperature.

The electrochemical measurements combined with spectroscopic analysis were carried out in an undivided three-electrode cell containing 20 cm³ of electrolyte. The solution was purged by Argon bubbling before the measurements and kept under Argon atmosphere during the measurements. The working electrode was a stainless steel (AISI 304) rod (Ø 0.8 cm) embedded in a Teflon holder. In order to perform reliable FT-IR measurements, the working surface of the rod was polished metallographically down to a mirror finish. This material was studied either as such (sample A) or coated by PANI (sample B), by PANI with $CNTs_c$ (sample C) and by PANI with $CNTs_{hm}$ (D). The counter electrode was a Pt ring coplanar with the steel working electrode. An external Pt quasi-reference electrode (QRE) was used, connected to the electrochemical cell through a capillary contact. The stability of the potential of the Pt QRE was proved by long-term measurements carried out in the relevant electrolyte against an Ag/AgCl reference electrode. All the potentials are reported versus Ag/AgCl. The applied potential was controlled by an AMEL 2049 potentiostat.

FT-IR measurements were carried out using a Nicolet NEXUS apparatus, equipped with an MCT-High D* detector cooled by liquid nitrogen. *p*-Polarised light was used, obtained with a ZnSe Au wire grid polariser. The beam path of the FT-IR spectrometer was continuously purged with a Parker Balston 75-52-12VDC CO_2 remover/air dryer system. The resolution of the spectrometer was set to 8 cm⁻¹. The spectra were acquired by means of Subtractively Normalised Interfacial FT-IR (SNIFTIR) procedure while the electrode potential was stepped between the reference potential E_1 and a variable sample potential E_2. In our experiments, a spectrum at the reference potential was measured immediately before the measurement at each studied potential. Each measurement consisted in collecting 128 interferograms and adding the respective Fourier-transforms. Each set of 128 averaged spectra was used to calculate the relative change of the electrode reflectivity, defined as $\Delta R/R = [R(E_2) - R(E_1)]/R(E_1)$, where $R(E_1)$ and $R(E_2)$ are the electrode reflectivity at the reference potential E_1 and at the sample potentials E_2, respectively. The reference spectrum was collected at $E_1 = -100$ mV and the series of spectra were measured by changing the potential starting from 1050 mV stepwise by 200 mV, in the anodic direction. An FT infrared reflection absorption spectra (FT-IRRAS) thin-layer device was employed for in situ working, as referred by some of the authors (Bozzini et al. 2004, 2006; Huerta et al. 2004). The working electrode was pressed against a CaF_2 prismatic 60° IR-window. The cell was located in the beam path of a VeeMax mirror system, with reflection angle set at 60°.

Results and discussion

Electrochemical co-deposition

The formation and deposition of PANI and PANI–CNTs films on carbon paper were obtained by means of three consecutive CV scans recorded from 0.0 to 1.2 V at a scan rate of 20 mV s⁻¹.

Figure 1 shows the first CV curves recorded during electrodeposition of PANI and when $0.3\%_{v/v}$ CNT_c and CNT_{hm} were introduced in aniline solution. The black curve is relative to the formation of the PANI film and shows an irreversible peak at about 1.1 V attributed to aniline oxidation. The grey and
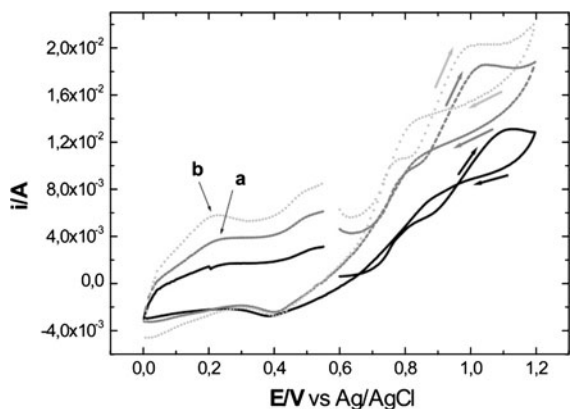
Fig. 1 Cyclic voltammograms of the first potential cycle on carbon paper substrate in aqueous solution 1 M HCl + 0.25 aniline dissoluted with different contents of CNTs: $0\%_{v/v}$ (*black line*), $0.3\%_{v/v}$ CNT_c (*grey line*) and $0.3\%_{v/v}$ CNT_{hm} (*light grey line*). Scan rate: 20 mV s^{-1}

light grey curves show the formation of PANI–CNTs composite films from an aniline solution containing CNT_c and CNT_{hm}, respectively. From an early comparison of the three curves, it is possible to notice that the voltammograms relative to the solutions containing CNT_c or CNT_{hm} are similar in shape to that recorded from the solution containing only aniline. However, the curves for PANI–CNTs exhibit a considerable increase in current intensities at the monomer oxidation region. Moreover, the CNTs addition to the aniline solution favours a catalytic effect towards the monomer oxidation. In fact the aniline is oxidised more readily in presence of CNTs (see the peak shifted at less anodic potential in Fig. 1), producing a higher current density during the anodic oxidation. This phenomenon was already observed by Wu et al. (2006), who reported that the presence of CNTs in an acid aniline aqueous solution accelerates the growth rate of PANI.

Furthermore, we observed a higher current when CNT_{hm} were used. This should be attributed to the different dimensional characteristics of the CNTs, such as diameter and length producing a different surface area. So, we suppose that the higher current density observed during the polymerisation process should be attributable to the wider surface area shown by the CNT_{hm}.

At the same time, for both CNTs-based composites, an anodic peak around 0.2 V appears. This peak can be explained trough two mechanistic theories proposed

by Huang et al. (2003). One possibility is that CNTs and aniline undergoes strong interactions and leads to charge stabilisation, promoting the protonation of PANI. The other is that CNTs act as condensation nuclei promoting the polymer aggregation.

A similar behaviour was observed in voltammograms recorded for lower CNTs content, but clearly the effect of CNTs presence is less considerable.

Figure 2 shows the CVs of the three cycles in 1 M HCl solution containing 0.25 M aniline and 0% CNTs (a), $0.3\%_{v/v}$ CNT_c (b) and $0.3\%_{v/v}$ CNT_{hm} (c), respectively. As previously described, in the first positive potential scan, the aniline is oxidised, exhibiting an irreversible anodic peak. This peak is at 1.1 V in absence of CNTs, whereas it is shifted at lower anodic potential, i.e. 1.0 V, in the presence of CNTs.

When the aniline is oxidised, the polymer growth process takes place. Voltammograms recorded during continuous scans showed an increasing current in each successive cycle, meaning the regular growth of the polymer film onto the carbon substrate.

Referring to Fig. 2b, c, during the subsequent scans in presence of CNTs, the oxidation of aniline occurs at lower potentials due to catalytic effect of PANI–CNTs deposited on the substrate during the first scan. The variation of the recorded current is due to the different typology of CNTs, as mentioned previously. At the same time, this result indicates that a higher amount of PANI was electrodeposited when CNTs were present in the solution.

Morphological characterisation

Before their use in aniline solution, CNTs were analysed by Scanning Electron Microscopy. In Fig. 3a and b SEM images of CNT_{hm} and CNT_c, respectively, are reported. They are like hollow ropes but the CNT_{hm} are clearly more curly and with a lower diameter than CNT_c. In point of chemical view, no relevant difference is appreciable between the two CNTs kinds, as demonstrated by C1s XPS peak (not reported here), acquired before and after the purification process.

After electrochemical co-deposition, the surface of all PANI-based films was examined by SEM. Figure 4 shows SEM images of the surface of pure PANI and PANI–CNT_c and PANI–CNT_{hm} films, respectively, deposited on carbon paper, when in the
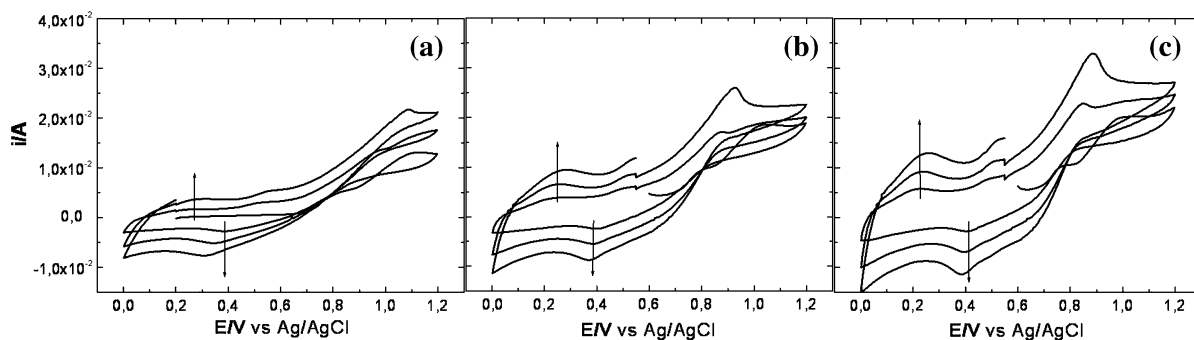
Fig. 2 Cyclic voltammograms comparing the electrochemical deposition of PANI (**a**), CNT$_c$/PANI (**b**) and CNT$_{hm}$/PANI (**c**) films from aqueous solution 1 M HCl + 0.25 M aniline dissoluted with different contents of CNTs: 0%$_{v/v}$ (**a**), 0.3%$_{v/v}$ CNT$_c$ (**b**) and 0.3%$_{v/v}$ CNT$_{hm}$ (**c**). Scan rate: 20 mV s^{-1}
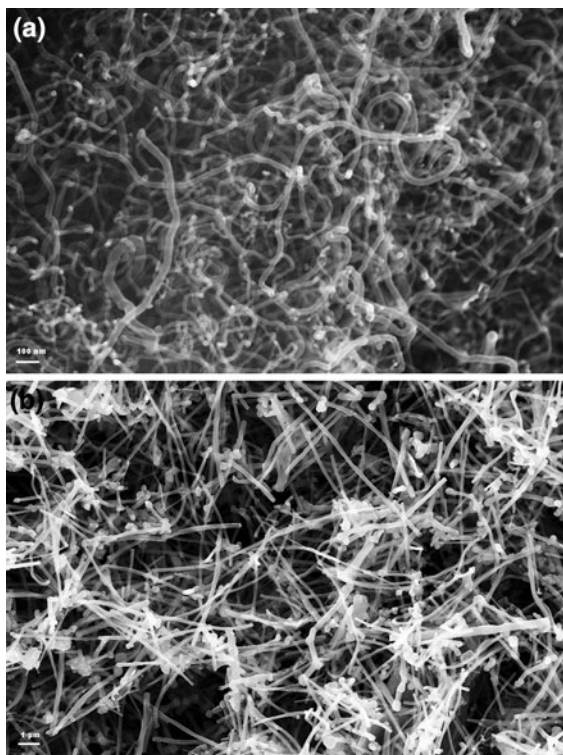
Fig. 3 SEM micrograph of CNT$_{hm}$ (**a**) and CNT$_c$ (**b**)

aniline solution the CNTs at the maximum concentration were present. The morphology of PANI deposit (Fig. 4a, b) is porous and appears composed of nano-fibrils. For the PANI–CNTs composites, the changes in the morphology are well-rendered in Fig. 4c–f. The diameter and the length of the fibrils in composite films are similar to those of individual CNT, meaning that PANI covered each CNT making a thin layer around it. In this way, the individual CNT acted as backbone to build the polymer. This fact can be confirmed also from some cracks evidenced on some fibrils (see arrows in Fig. 4d–f). In particular, when CNT$_c$ were used, PANI fibrils appear more straightened and with ends chopped, so they remind the CNT shape. In case of CNT$_{hm}$, the morphology of CNT is not so easily recognised under the PANI layer, but equally it is possible to highlight a different shape of PANI–CNTs fibrils.

From these observations and from the cited considerations reported by other groups (Zengin et al. 2002; Cochet et al. 2001; Peng et al. 2007), we could deduce that the interaction between CNTs and PANI produced a PANI coating on each CNT or CNTs wisp. The amount of PANI covering CNTs could depend on the exposed area of CNTs and therefore also on their morphological and structural characteristics that are hardly quantifiable.

Electrochemical characterisation

Electrochemical characterisation of PANI and PANI–CNTs films was carried out by CV in 0.5 M H$_2$SO$_4$, in presence of Argon gas. Figure 5a and b shows the electrochemical characterisation of three coatings: PANI, 0.1%$_{v/v}$ CNTs–PANI and 0.3%$_{v/v}$ CNTs–PANI for CNT$_{hm}$ and CNT$_c$, respectively. The PANI–CNT$_{hm}$ and PANI–CNT$_c$ voltammograms show the same behaviour even if a lower current density is recorded in the case of the composite CNT$_c$-based.
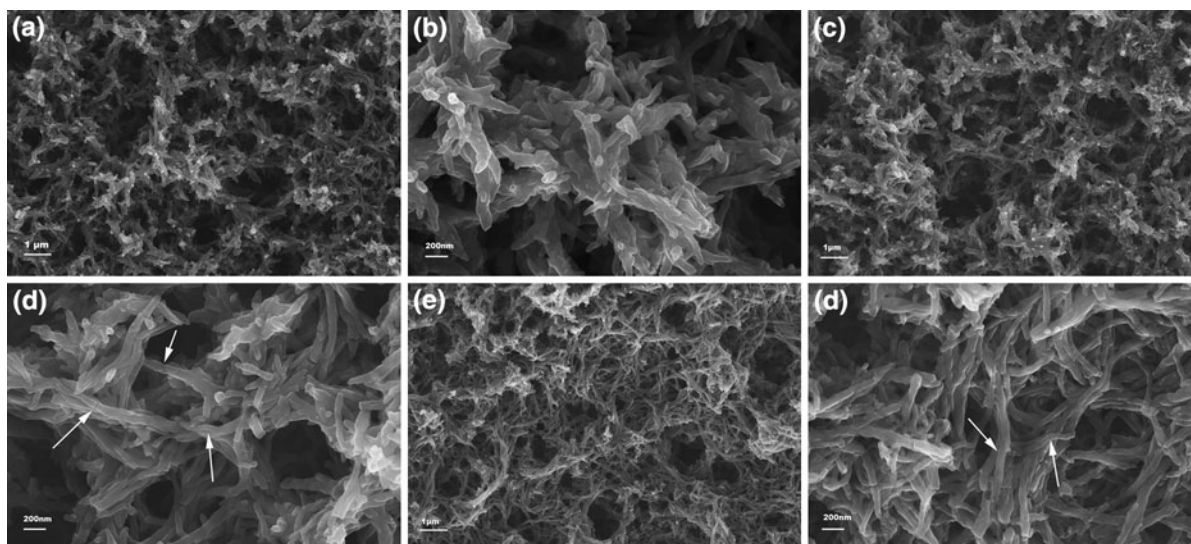
Fig. 4 SEM images of the surface of PANI and CNTs/PANI composite films: PANI (**a**, **b**), 0.3%$_{v/v}$ CNT$_c$/PANI (**c**, **d**) and 0.3%$_{v/v}$ CNT$_{hm}$/PANI (**e**, **f**)

The peaks structure conforms to that already proven in literature (Stilwell and Park 1989). The anodic peak A at about 0.25 V represents the transition from leucoemeraldine to protonated emeraldine, which is known to be the most conductive of the different forms of PANI. Peak B at about 0.95 V corresponds to the most oxidised state of PANI, concerning the oxidation of emeraldine to pernigraniline. The peaks A′ and B′ during the cathodic scan correspond to the reversal process.

No additional peaks can be observed due to the CNTs presence in the CV curves, indicating the absence of electrochemical activity of CNTs. However, when are compared with PANI, the peaks intensities for PANI–CNTs films are higher, especially for PANI containing CNT$_{hm}$. This result agrees with the hypothesis that the amount of electrodeposited PANI increases when CNTs are present in the solution. This could allow to have an improvement of the electrochemical activity of the composite films compared with the pristine PANI. This aspect will be the subject of further investigations.

Figure 6a shows the last of 10 voltammograms acquired in 0.5 M H$_2$SO$_4$ on films of PANI and PANI containing 0.3%$_{v/v}$ CNT$_{hm}$ and 0.3%$_{v/v}$ CNT$_c$. An anodic shift is found on the anodic peaks and a cathodic shift on the cathodic ones, again correlating with the CNTs concentration in the solution. The shift

in the redox peaks can be explained in terms of the effect on the CNTs addition to the electronic structure of PANI. In fact, the created interaction between CNTs and PANI, represented in Scheme 1, can inhibit the total PANI protonation in H$^+$ ions presence, and therefore makes it more possible to block the transition of quinonoid imine (=N–) to benzenoid amine (–NH–).

In Fig. 6b, the CVs recorded after FeSO$_4$ injection into the H$_2$SO$_4$ solution are reported. The CV corresponding to PANI without incorporating CNTs in H$_2$SO$_4$ (dot-dashed line) is also shown for comparison. The injection of FeSO$_4$ gives rise to an evident change in the voltammetric behaviour. It can be noticed that A- and B-type peaks are progressively shifted and their relative intensities are changed. This result can be related to the competition between Fe^{2+} and H$^+$ for protonation sites and gives information on the ion-exchange capability of PANI. Ion-exchange behaviour of PANI has been pinpointed as one of the chief effects leading to the corrosion protection of ferrous alloys by PANI layers (Wang 2002; Biallozor and Kupniewska 2005). As a consequence, the enhancement of the peak shift brought about by the incorporation of CNTs into PANI layers suggests that CNTs favour the interaction of Fe^{2+} with the modified PANI film, possibly leading to an improved blocking of the products of the corrosion reaction.
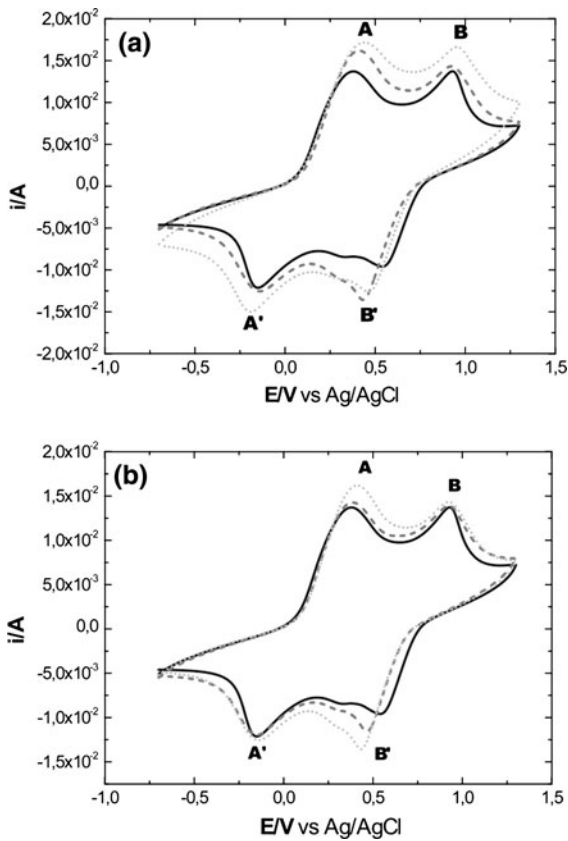
Fig. 5 Cyclic voltammograms of the first potential cycle in 0.5 M H_2SO_4 of different PANI films containing CNTs: $0\%_{v/v}$ (*black line*), $0.1\%_{v/v}$ CNT_{hm} (*grey line*) and $0.3\%_{v/v}$ CNT_{hm} (*light grey line*) (**a**) and $0\%_{v/v}$ (*black line*), $0.1\%_{v/v}$ CNT_c (*grey line*) and $0.3\%_{v/v}$ CNT_c (*light grey line*) (**b**). Scan rate: 50 mV s^{-1}

Fig. 6 Cyclic voltammograms after 10 CVs (**a**) and 10 mM $FeSO_4$ (**b**) in 0.5 M H_2SO_4 of different PANI films containing CNTs: $0\%_{v/v}$ (*black line*), $0.3\%_{v/v}$ CNT_c (*grey line*) and $0.3\%_{v/v}$ CNT_{hm} (*light grey line*). Scan rate: 50 mV s^{-1}

Potentiodynamic measurements

In order to assess the anodic performance of the investigated materials, potentiodynamic scans were measured in an ethyl alcohol solution containing H_2SO_4 (Fig. 7). These integral measurements have been performed in the spectroelectrochemical cell with the working electrode lifted above the CaF_2 optical window, according to the procedure recommended in (Tadjeddine and Le Rille 1999). The typical ethanol oxidation peak can be noticed (Bozzini et al. 2010a, b), followed by an anodic current density increase, mainly related to the oxygen evolution reaction. It is not straightforward to draw conclusions regarding the corrosion resistance of the metal substrate only from these potentiodynamic scans, because the anodic current density background
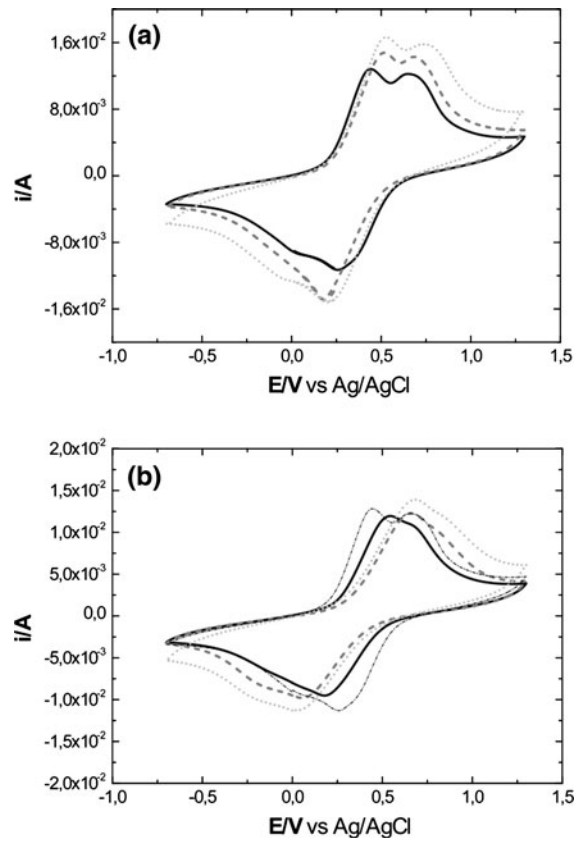
corresponds to ethanol and water oxidation. However, we reported an interpretation of the acquired curves.

Bare (A) and PANI-coated AISI 304 (B) show similar activities towards ethanol oxidation, with a slightly lower activation overvoltage in the presence of the PANI film. The addition of CNTs shifts the oxidation threshold towards higher potentials, denoting an inhibiting effect. We attributed the differences in the absolute values of the current density to the different effective surface areas of the different coatings.

We decided to measure potential-dependent in situ FTIR spectra to gain a great insight of the anodic behaviour of these materials, to assess the corrosion performance of the uncoated and coated stainless steel and to obtain molecular-level information on the electrocatalytic behaviour of the composite coating. It is worth noting that this seems to be the first in situ
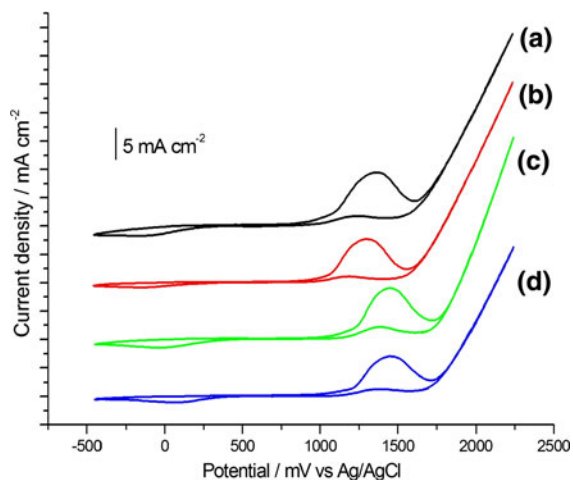
Fig. 7 Potentiodynamic curves measured at AISI 304 electrodes without (*A*) and with the following coatings: (*B*) PANI, (*C*) PANI coating containing CNT_c, (*D*) PANI coating containing CNT_{hm} in contact with a 50 mM H_2SO_4, 50 vol% ethanol aqueous solution. Scan rate: 100 mV s^{-1}

electrochemical FTIR investigation performed at a stainless steel electrode.

In situ FTIR spectroelectrochemistry

In Figs. 8, 9, 10 and 11, the potential-dependent FTIR spectra measured for the four investigated systems are reported. The release of Fe-group corrosion products can be studied by in situ FTIR (Bozzini et al. 2010b). In the present case, the expected corrosion product of AISI 304 is Fe^{2+}, typically in the form of a hydroxide. At relevant potentials these species are predisposed to oxidise further to Fe^{3+}. The OH stretching bands of the hydroxide at ca. 3700 cm^{-1} and bending modes of FeOOH at ca. 1140 cm^{-1} have therefore been reported to be indicative of the build up of Fe^{2+} and Fe^{3+} in the electrolyte, respectively (Iwasita and Nart 1995).

The bare AISI 304 electrode (sample A, Fig. 8) exhibits the formation of Fe^{2+} for potentials of 1250 mV and higher. A notable increase in the amount of Fe^{3+} present in the electrolyte can be detected at 2050 mV. In presence of PANI coating on AISI 304 (sample B, Fig. 9), the inception of Fe oxidation is shifted to 1450 mV, with simultaneous formation of Fe^{2+} and Fe^{3+}, coherently with thermodynamic data. Moreover, the amount of released corrosion products is reduced. The addition of $CNTs_c$

(sample C, Fig. 10) and $CNTs_{hm}$ (sample D, Fig. 11) moves the Fe oxidation threshold as high as 2250 mV, considerably enhancing the corrosion protection effect of the coating. The only measurable difference between the two types of CNTs is that the Fe^{2+} band at 2250 mV is five times larger when the $CNTs_{hm}$ are present with respect to $CNTs_c$.

As far as the vibrational structure of PANI or CNTs, no spectral features corresponding to some variations could be detected when the potential varied. Nevertheless, by comparing the direct spectra of samples B and A (plot α) and C or D (yielding the same results) and B (plot β), typical bands of PANI and CNTs could be observed (Fig. 12). In the wave number range 1450 ÷ 1600 cm^{-1} (plot α) typical PANI modes (benzenoid and quinoid phenyl ring) are present (Bozzini et al. 2007, Bozzini and Fanigliulo 2002), and at 1730 cm^{-1} (plot β) the C=O stretching of carboxyl groups, being diagnostic for CNTs (Dhand et al. 2008), is visible.

In order to investigate the protective corrosion behaviour of PANI and PANI–CNTs coatings with respect to the corrosive products of the ethanol oxidation, in situ FTIR investigations were also conducted in presence of pure ethanol when the potential varied. The following bands can be regarded as diagnostic in the present case (Bozzini et at. 2010b): (i) ca. 1280 cm^{-1} C–OH stretching of acetic acid; (ii) ca. 1360 cm^{-1} coupled C–O stretching and OH deformation of ethanol; (iii) stretching of linearly adsorbed CO (ca. 1920 cm^{-1}); (iv) ca. 2980–2900 cm^{-1} methyl and methylene stretching bands.

Ethanol is oxidised at the bare AISI 304 electrode (sample A, Fig. 8) in the whole investigated potential range. In particular, oxidative adsorption of ethanol with formation of adsorbed CO is found between 1050 and 1850 mV, while at higher potentials (2050 and 2250 mV) CO is oxidatively desorbed with formation of CO_2.

In the presence of a PANI coating (sample B, Fig. 9), the spectral features corresponding to the bulk ethanol oxidation are notably enhanced and the adsorption of inhibiting CO seems less favoured. In particular, at 1050 mV ethanol seems to adsorb without reacting (neither CO nor acetic acid band can be measured). Oxidative adsorption is found at 1250 mV and the bulk oxidation seems to prevail in the range 1450 ÷ 1850 mV until the CO_{ads} peak disappears, whereas an oxidative desorption yields CO_2 at 2250 mV.

Fig. 8 In situ FTIR spectra measured at an AISI 304 electrode (sample A) in contact with a 50 mM H_2SO_4, 50 vol% ethanol aqueous solution at the indicated potentials
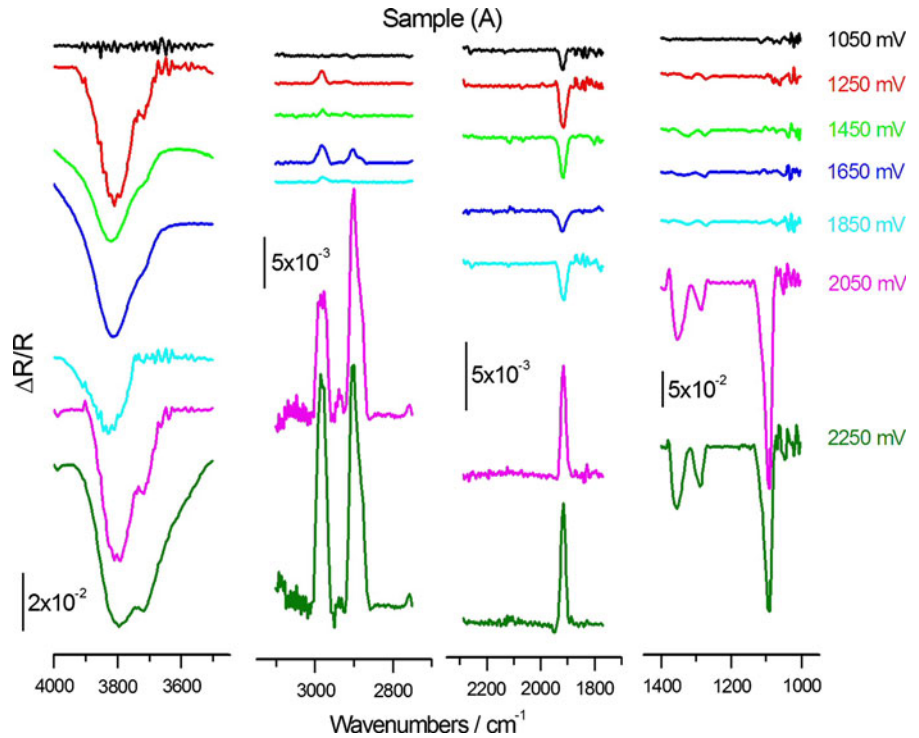

Fig. 9 In situ FTIR spectra measured at a PANI-coated AISI 304 electrode (sample B) in contact with a 50 mM H_2SO_4, 50 vol% ethanol aqueous solution at the indicated potentials
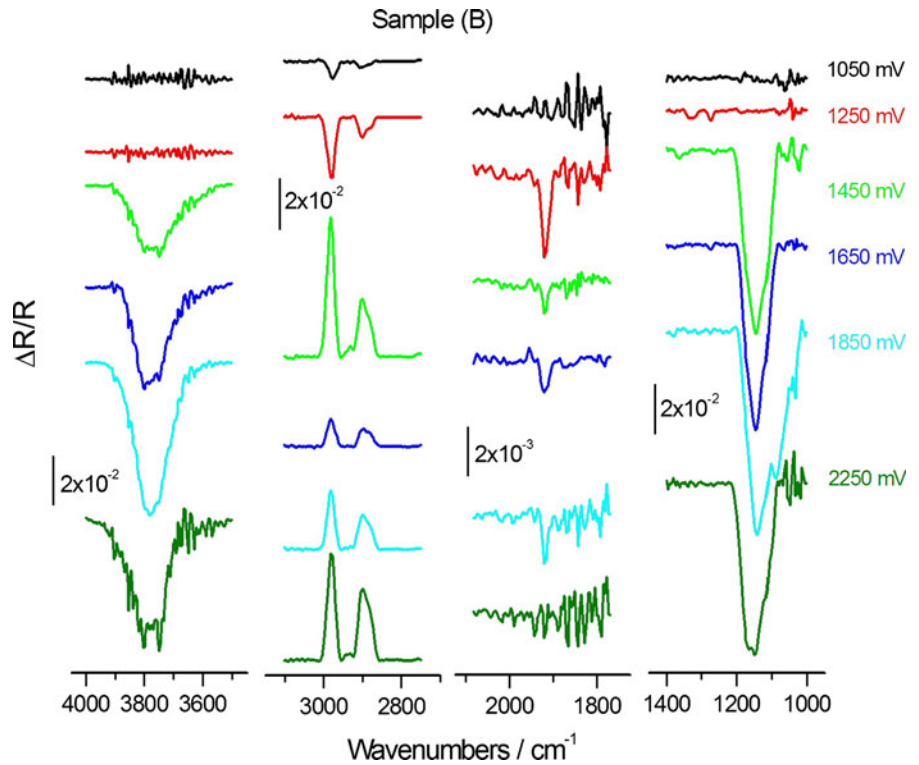
Fig. 10 In situ FTIR spectra measured at an AISI 304 electrode coated with PANI coating containing CNT_c (sample C) in contact with a 50 mM H_2SO_4, 50 vol% ethanol aqueous solution at the indicated potentials
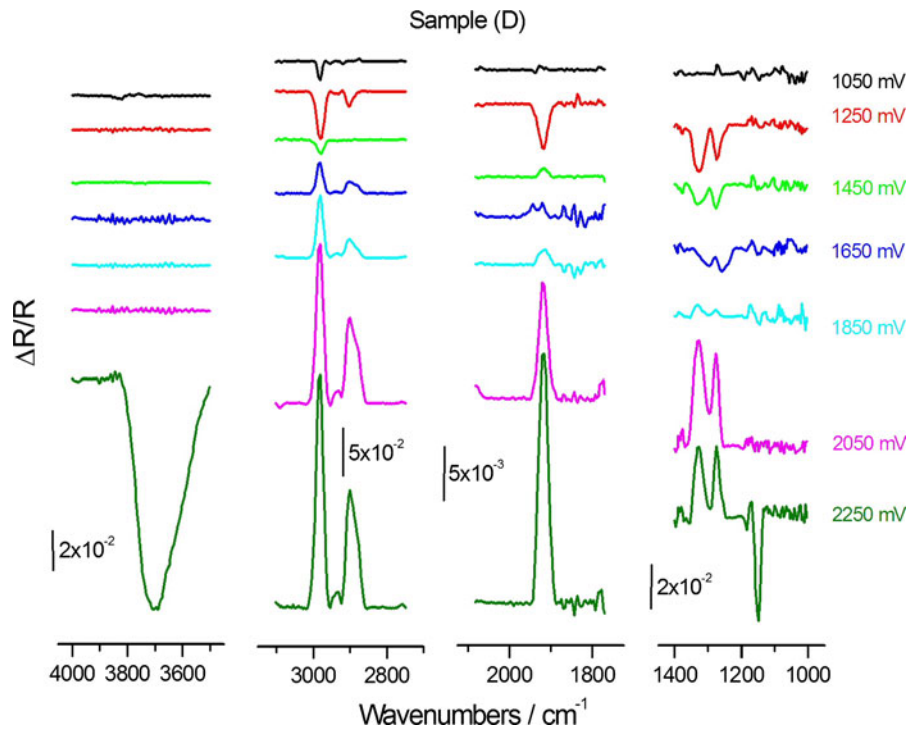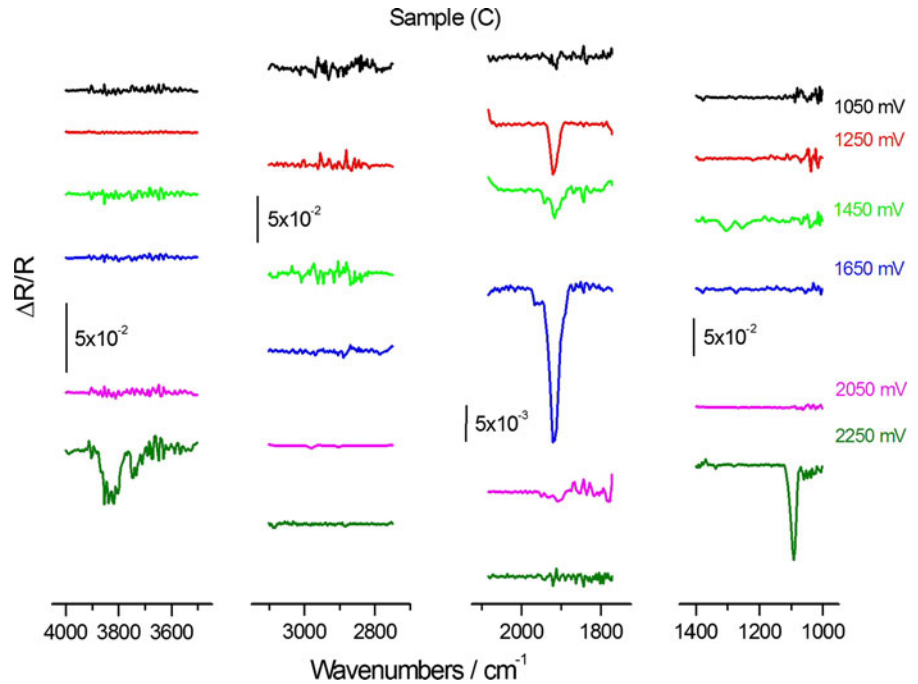

Fig. 11 In situ FTIR spectra measured at an AISI 304 electrode coated with PANI coating containing CNT_{hm} (sample D) in contact with a 50 mM H_2SO_4, 50 vol% ethanol aqueous solution at the indicated potentials

Fig. 12 Ratios of FTIR spectra measured with bare AISI 304 (sample A), PANI coating (sample B) and PANI containing CNT_c (sample C). Plot α: B (1200 mV)/A (1200 mV); plot β: C (1200 mV)/B (1200 mV)
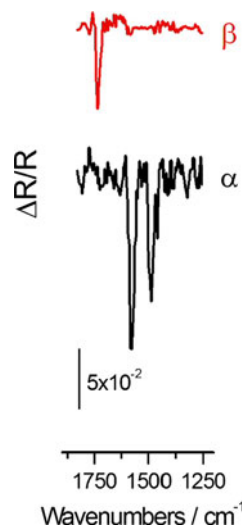
Composite coatings with dispersion of CNT_c into PANI (sample C, Fig. 10) show hardly measurable bulk ethanol peaks. In fact, no evidence of CO adsorption is found at 1050 mV, while a negative CO_{ads} band can be measured in the interval $1250 \div 1650$ mV. This phenomenon grows with applied potential and it vanishes at 2050 mV. The absence of bulk consumption bands and of positive CO_{ads} peaks at high anodic potentials suggests that the electrode surface is blocked, probably by strongly adsorbed CO. In this respect, at the highest investigated potentials (2050 and 2250 mV) neither bulk nor surface modes are visible. This fact can be attributed to the serial correlation effects, due to the recurrence of measurements made alternating the reference and the current potential. In fact, when a strong adsorption occurs, the interfacial composition would not change, resulting in a featureless differential spectrum.

Composite coatings with CNT_{hm} (sample D, Fig. 11) exhibit the oxidative adsorption of ethanol at 1250 mV. At potentials in the range $1450 \div 1850$ mV, relatively weak positive methyl and methylene stretching peaks, a small positive CO_{ads} band and relatively strong acetic acid peaks are present. This suggests that ethanol oxidation goes on more efficiently than in the presence of CNT_c. At 2050 and 2250 mV, the consumption of ethanol in the bulk seems to increase notably and positive CO_{ads} bands attest the oxidative desorption of this species. It is worth noting that the maximum of the CO_{ads} band exhibits a low value with a small and negative Stark tuning. This fact suggests that the charge-

transfer between the substrate and the adsorbate is much lower than in the case of noble metals or Pt-group metal-based catalysts so that a non-standard mechanism seems to be operative in these systems. This point is worth further investigation. The Stark shift is linear at low applied anodic potentials and it tends to reach an asymptote, due to classical field-confinement effects (Iwasita and Nart 1995). The following values have been estimated from the data points belonging to the linear part: (A) 4.46 ± 0.24 cm^{-1} V^{-1}; (B) 5.52 ± 1.05 cm^{-1} V^{-1}; (C) 7.40 ± 0.62 cm^{-1} V^{-1}; (D) 3.32 ± 0.68 cm^{-1} V^{-1}.

The behaviour of the investigated materials in H_2SO_4 solution can be simply rationalised according to a simple scheme, discussed below. (i) At the bare metal electrode, the potential drop is entirely located at the metal–electrolyte interface. (ii) At the PANI coated electrode, assuming a high perfection of the coating and a high electronic conductivity, the potential drop is located at the PANI–electrolyte interface. In this simple view, the metal being below is electrochemically inactive and consequently protected from corrosion. (iii) In the presence of CNTs, the electronic conductivity of the coating is expected to be increased and parallel conductive paths across the composite film can develop. In this case, the metal is screened as in case (ii).

Conclusions

Electrochemical deposition of polyaniline (PANI) and PANI containing two different types of CNTs was carried out on carbon paper and stainless steel substrates. The electrochemistry of the films was investigated by cyclic voltammetry. The results suggested that the addition of CNTs in the polymer matrix allowed to increase the amount of polyaniline electropolymerised on the substrate.

The morphological characterisation of these new composite materials showed the polymer was electrogenerated onto the CNTs surface acting as backbone. The incorporation of CNTs in PANI films occured during the electrogeneration of PANI. The cause could be the donor–acceptor effect created between CNT and PANI.

In terms of the functional behaviour, the electrochemical characterisation of composite coatings in presence of $FeSO_4$ demonstrated the capability of the

composite material to interact with Fe^{2+}, so showing the film potential to block the products of the AISI 304 corrosion.

From FTIR measurements the following conclusions can be argued: (i) PANI and PANI–CNTs films exhibit a notable corrosion protection action for AISI 304 in sulphuric acid solution. This property is further enhanced by the addition of CNTs. (ii) by comparing the composite with the two kinds of CNTs, the coating with $CNTs_c$ has a better performance in term both of ethanol oxidation and obstacle for the diffusion of corrosion products to the substrate, in spite of the hypothesised higher amount of PANI deposited onto $CNTs_{hm}$. This aspect needs further investigations.

As the PANI–CNTs/films show better anticorrosion properties than PANI, they could be suitable as protective coatings on electrode materials for new electronic devices.

References

Biallozor S, Kupniewska A (2005) Conducting polymers electrodeposited on active metals. Synth Met 155:443–449. doi:10.1016/j.synthmet.2005.09.002

Bozzini B, Fanigliulo A (2002) Effects of Tl on the electrocrystallisation of thick Au layers from KAu(CN)2 solutions. J Cryst Growth 243:190–203 PII: S002202480201 4318

Bozzini B, Mele C, Tadjeddine A (2004) Electrochemical adsorption of cyanide on Ag(1 1 1) in the presence of cetylpyridinium chloride. J Cryst Growth 271:274–286. doi:10.1016/j.jcrysgro.2004.07.063

Bozzini B, Giovannelli G, Mele C, Brunella F, Goidanich S, Pedeferri P (2006) An investigation into the corrosion of Ag coins from the Greek colonies of Southern Italy. Part I: an in situ FT-IR and ERS investigation of the behavior of Ag in contact with aqueous solutions containing 4-cyanopyridine. Corros Sci 48:193–208. doi:10.1016/j.corsci.2004.11.024

Bozzini B, Mele C, Romanello V (2007) An in situ FT-IR evaluation of candidate organic corrosion inhibitors for carbon steel in contact with alkaline aqueous solutions. Mater Corros 58:362–368. doi:10.1002/maco.200604015

Bozzini B, De Gaudenzi GP, Busson B, Humbert Ch, Six C, Gayral A, Tadjeddine A (2010a) In situ spectroelectrochemical measurements during the electro-oxidation of ethanol on WC-supported Pt-black, based on sum-frequency generation spectroscopy. J Power Sour 195:4119–4123. doi:10.1016/j.jpowsour.2010.01.017

Bozzini B, De Gaudenzi GP, Tadjeddine A (2010b) In situ spectroelectrochemical measurements during the electro-oxidation of ethanol on WC-supported Pt-black. Part II: monitoring of catalyst aging by in situ Fourier transform infrared spectroscopy. J Power Sources 195:7968–7973. doi:10.1016/j.jpowsour.2010.06.019

Cochet M, Masser WK, Benito AM, Callejas MA, Martinèz MT, Benoit JM, Schreiber J, Chauvet O (2001) Synthesis of a new polyaniline/nanotube composite: "in situ" polymerisation and charge transfer through site-selective interaction. Chem Commun 16:1450–1451. doi:10.1039/b104009j

Dhand C, Arya SK, Singh SP, Singh BP, Datta M, Malhotra BD (2008) Preparation of polyaniline/multiwalled carbon nanotube composite by novel electrophoretic route. Carbon 46:1727–1735. doi:10.1016/j.carbon.2008.07.028

Dikonimos Th, Giorgi L, Giorgi R, Lisi N, Salernitano E (2005) CNT growth on alumina supported nickel catalyst by thermal CVD. Diam. Rel. Mat 14:815–819. doi:10.1016/j.diamond.2004.11.001

Huang WS, Humphrey BD, MacDiarmid AG (1986) Polyaniline, a novel conducting polymer. Morphology and chemistry of its oxidation and reduction in aqueous electrolytes. J Chem Soc Faraday Trans 1 Phys Chem Condensed Phases 82: 2385–2400. doi:10.1039/F19868202385

Huang JE, Li XH, Xu JC, Li HL (2003) Well-dispersed single-walled carbon nanotube/polyaniline composite films. Carbon 41:2731–2736. doi:10.1016/S0008-6223(03)00359-2

Huerta F, Mele C, Bozzini B, Morallon E (2004) Voltammetric and in situ FTIRS study on CN- and Au(CN)x—complexes at the polycrystalline gold surface in citrate medium. J Electroanal Chem 569:53–60. doi:10.1016/j.jelechem.2004.02.013

Iwasita T, Nart FC (1995) In situ Fourier Transform Infrared Spectroscopy: a tool to characterize the metal-electrolyte interface at a molecular level. In: Gerischer H, Tobias CW (eds) Advances in electrochemical science and engineering, vol 4. VCH, Weinheim, pp 209–212

MacDiarmid AG, Epstein AJ (1995) Secondary doping in polyaniline. Synth Met 69:85–92. doi:10.1016/0379-6779(94)02374-8

MacDiarmid AG, Chiang JC, Richter AF, Epstein AJ (1987) Polyaniline: a new concept in conducting polymers. Synth. Met 18:285–290. doi:10.1016/0379-6779(87)90893-9

Peng C, Jin J, Chen GZ (2007) A comparative study on electrochemical co-deposition and capacitance of composite films of conducting polymers and carbon nanotubes. Electrochim Acta 53:525–537. doi:10.1016/j.electacta.2007.07.004

Qian D, Dickey EC, Andrews R, Rantell T (2000) Load transfer and deformation mechanisms in carbon nanotube-polystyrene composites. Appl Phys Lett 76:2868–2870. doi:10.1063/1.126500

Skotheim TJ, Elsenbaumer RL, Reynolds JR (1998) Handbook of conducting polymers. Marcel Dekker, New York

Stilwell DE, Park SM (1989) Electrochemistry of conductive polymers. J Electrochem Soc 135:433–2491. doi:10.1016/0379-6779(89)90293-2

Sun Y, Wilson SR, Schuster DI (2001) High dissolution and strong light emission of carbon nanotubes in aromatic amine solvents. J Am Chem Soc 123:5348–5349. doi:10.1021/ja0041730

Tadjeddine A, Le Rille A (1999) Sum and difference frequency generation at electrode surfaces. In: Wieckowski A (ed) Interfacial electrochemistry. Dekker, New York, pp 317–343

Wagner HD, Lourie O, Feldma Y, Tenne R (1998) Stress-induced fragmentation of multiwall carbon nanotubes in a polymer matrix. Appl Phys Lett 72:188–190. doi:10.1063/1.120680

Wang J (2002) Polyaniline coatings: anionic membrane nature and bipolar structures for anticorrosion. Synth Met 132:3–56 PII: S0379677902002047

Wu G, Li L, Li JH, Xu BQ (2006) Methanol electrooxidation on Pt particles dispersed into PANI/SWNT composite films. J Power Sources 155:118–127. doi:10.1016/j.jpowsour.2005.04.035

Zengin H, Zhou W, Jin JY, Czerw R, Smith DW, Echegoyen L, Carroll DL, Foulger SH, Battato J (2002) Carbon nanotube doped polyaniline. Adv Mater 14:1480–1483. doi:10.1002/1521-4095(20021016)